Robust 3D scalar imaging condition for elastic RTM

Yuting Duan, presently at Shell International Exploration and Production Inc., formerly at Center for Wave Phenomena, Colorado School of Mines
Paul Sava, Center for Wave Phenomena, Colorado School of Mines

SUMMARY

We propose an elastic scalar imaging condition that corrects for the polarity change; however, this imaging condition requires additional prior information which may not be known accurately, or may suffer from interference of waves propagating from opposite sides of a reflector. Using incorrect P- and S-mode velocities causes reflectors in migrated PP, PS, and SP images to be shifted from their true positions. We show that it is more reliable to estimate reflector normals from PS and SP images, computed using conventional imaging methods, instead of from PP images. We also demonstrate that the PS and SP images computed using our elastic imaging condition for waves propagating from opposite sides of a reflector have the same polarity, and therefore they can be stacked over experiments without canceling each other. This analysis, illustrated with numeric experiments, demonstrates the intrinsic robustness of our elastic scalar imaging condition.

INTRODUCTION

Conventional seismic data processing is typically based on the acoustic wave equation, and thus uses compressional waves while regarding shear waves as noise. Ongoing improvements in computational capability and seismic acquisition have made imaging using multi-component elastic waves feasible. Multi-component seismic data can provide additional subsurface information, such as fracture distributions and elastic properties (MacLeod et al., 1999; Mehta et al., 2009; Sen, 2009).

For elastic reverse-time migration, the constructed vector wavefields allow for a variety of imaging conditions (Yan and Sava, 2008; Denli and Huang, 2008; Artman et al., 2009; Wu et al., 2010). One widely used imaging condition is crosscorrelation of separated wave modes from the source and receiver wavefields, which yields PP, PS, SP, and SS images. However, because PS and SP reflectivities change signs at certain incidence angles, the computed PS and SP images change polarities at the corresponding angles.

Duan and Sava (2014) propose an imaging condition for elastic reverse-time migration, generating PS and SP scalar images with consistent polarity information for all experiments. This imaging condition requires additional information, i.e. the reflector normal field. Here, we investigate two practical problems associated with this imaging condition, including the estimation of the reflector normals when the reflectors are imaged at incorrect positions, and the imaging of a reflector by waves arriving from opposite sides.

ELASTIC SCALAR IMAGING CONDITION

Reconstructed source and receiver wavefields typically are decomposed into P- and S-modes prior to application of an imaging condition (Dellinger and Etgen, 1990; Yan and Sava, 2008). In isotropic media, by using Helmholtz decomposition, we obtain the P- and S-modes:

$$P = \nabla \cdot \mathbf{u}\,, \tag{1}$$

$$\mathbf{S} = \nabla \times \mathbf{u}\,. \tag{2}$$

Here, $P(e,\mathbf{x},t)$ and $\mathbf{S}(e,\mathbf{x},t)$ are functions of the experiment index e, space coordinate $\mathbf{x}$, and time t, and they represent the scalar P- and vector S-modes, respectively.

Duan and Sava (2014) propose alternative imaging conditions that result in scalar PS and SP images:

$$I^{PS} = \sum_{e,t} (\nabla P \times \mathbf{n}) \cdot \mathbf{S}\,, \tag{3}$$

$$I^{SP} = \sum_{e,t} (\nabla \times \mathbf{S} \cdot \mathbf{n})\, P\,. \tag{4}$$

The PS and SP scalar images are denoted by $I^{PS}(\mathbf{x})$ and $I^{SP}(\mathbf{x})$, respectively, and $\mathbf{n}(\mathbf{x})$ is a unit vector indicating the reflector normal and is assumed as prior information. This imaging condition is referred to as the elastic scalar imaging condition.

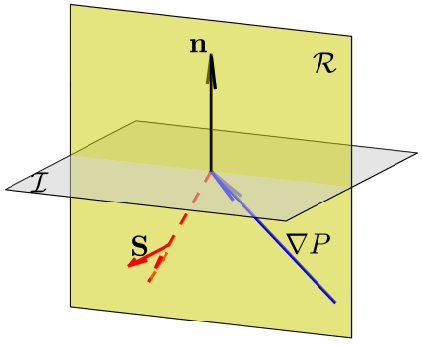

Figure 1: Schematic representation of reflection at an interface.

For the PS imaging condition (equation 3), vector ∇P is parallel to the propagation direction of the incident P-mode, as seen in Figure 1. The cross product of ∇P and normal vector $\mathbf{n}$ forms a vector orthogonal to the reflection plane $\mathscr{R}$, but parallel to vector $\mathbf{S}$, which is the polarization direction of the reflected S-mode. When the incidence angle changes sign, and the S-mode consequently change sign, vector $\nabla P \times \mathbf{n}$ reverses direction, thus compensating for the opposite polarization of the reflected S-mode. Therefore, we could obtain PS image without polarity reversal. There is a similar physical interpretation for the SP imaging condition (equation 4).

However, in practice, it is not realistic to obtain the true model, and the reflectors may be imaged at various positions in PP, PS, and SP images. In the following section, we show a robust way to estimate the reflector normal for imaging converted wave-modes.

ESTIMATION OF THE REFLECTOR NORMAL

The scalar imaging condition requires an estimate of the reflector normal **n**. If the velocity is incorrect, the reflectors in PP, PS, and SP images are incorrectly positioned, and it is inaccurate to estimate the normal for PS and SP imaging from the PP image. Reflector normals estimated from a PP image are inconsistent with those from a PS image and thus are unavailable for the scalar imaging condition. Therefore, instead of estimating reflector normals from a PP image, we choose to estimate the normal vectors from the PS image computed using the conventional imaging condition. Because the polarity reversal present in conventional PS images results in poor resolution of the stacked conventional PS image, we apply a simple correction for this polarity change, for example, by reversing the sign of the image at negative offsets.

We illustrate our approach using a modified Marmousi model (Versteeg, 1991, 1993), as shown in Figure 2a. Compared with the original model, we increase the depth of the water layer in order to generate PS conversion from a hard water bottom. Twenty explosive sources are evenly distributed along the surface, and 600 multicomponent receivers are located at depth $z = 0.05$ km. The source function is a Ricker wavelet with a peak frequency of 35 Hz. Cross-correlating the source P wavefield with the receiver P and S wavefields, we obtain the PP (Figure 2b) and PS (Figure 3a) images, respectively. For the PS image in Figure 3a, we apply a simple polarity correction by reversing the sign of the pre-stacked PS images at negative source-receiver offsets. Because the P- and S-velocities used for migration are 12% higher and 4% lower than the true model, respectively, the reflectors are at different positions in PP and PS image. With the reflector normal (Figure 2c) estimated from the PP image we compute the PS images using the scalar imaging condition (seen in Figure 2d). Notice that a reflector changes polarity at $(1.1, 0.7)$ km. If we estimate the reflector normal (Figure 3b) using the conventional PS image, we obtain a stacked PS image without distortion caused by polarity reversals.

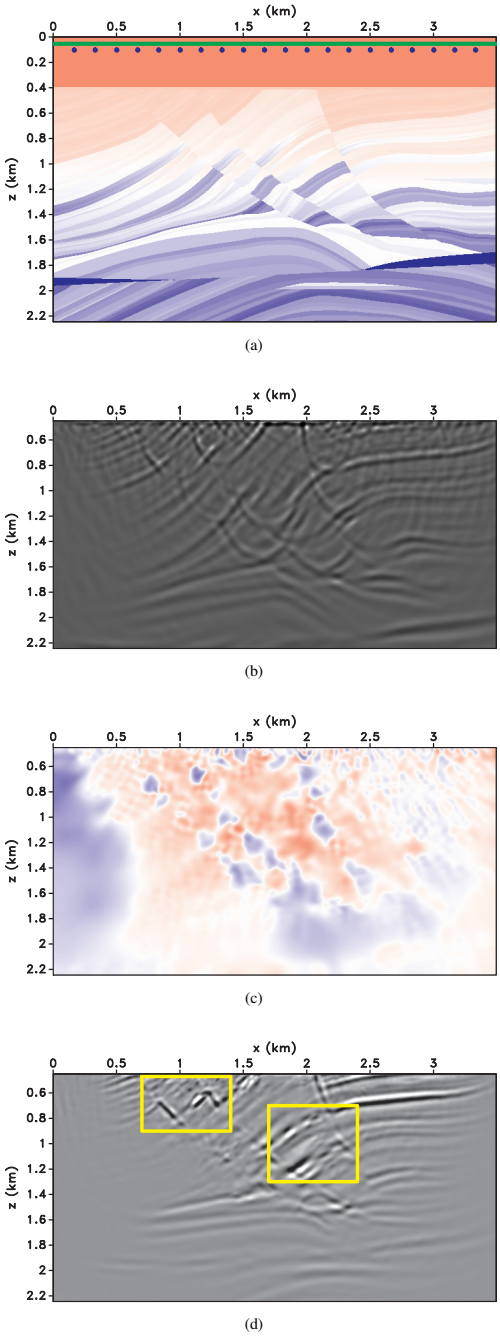

Figure 2: (a) The Marmousi model. (b) The stacked PP image computed by cross-correlating P-waves in source and receiver wavefields. (c) The reflector normal estimated using the PP image. (d) The PS image computed using the dip field from panel (b). The reflectors highlighted by the boxes are not continuous and poorly imaged.

IMAGING FROM OPPOSITE SIDES OF A REFLECTOR

In complex subsurface models, reflectors are often illuminated by waves approaching from opposite sides; e.g., a reflector might be imaged both from above by a down-going direct wave and from below by a diving wave. Consider the cases shown in Figures 1 and 4, depicting down-going and up-going PS converted waves, respectively. Assuming the incident P-modes in Figures 1 and 4 have the same polarity, then vectors ∇P point in opposite directions, and the reflected S-modes must have opposite polarities because reflectivity changes sign for incident waves approaching a reflector from opposite sides (Aki and Richards, 2002). Therefore, conventional PS images computed by migrating waves reflected off opposite sides of a reflector also have opposite polarities.

In contrast, the polarities of PS images computed using our

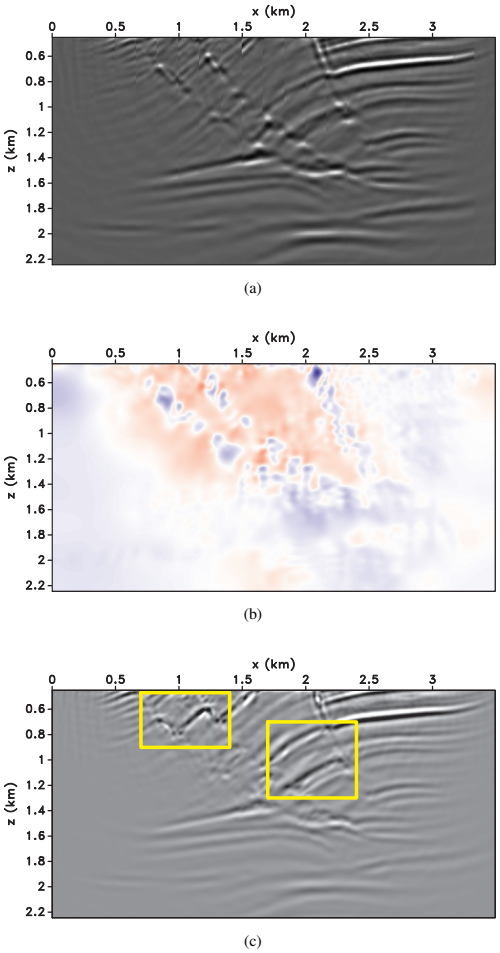

Figure 3: (a) The stacked PS image computed using the conventional imaging condition. The PS image polarity for individual shots are corrected by reversing the image at negative offsets. (b) The reflector dip estimated using PS image. (c) The PS image computed using the dip field. The reflectors highlighted by the boxes are better imaged compared to the PS image in Figure 2d.

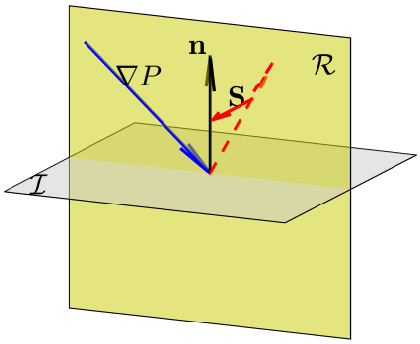

Figure 4: Schematic representation of reflection at an interface for up-going PS converted-modes. Compared to Figure 1, vector ∇P changes sign, resulting in the sign change of $\nabla P \times \mathbf{n}$.

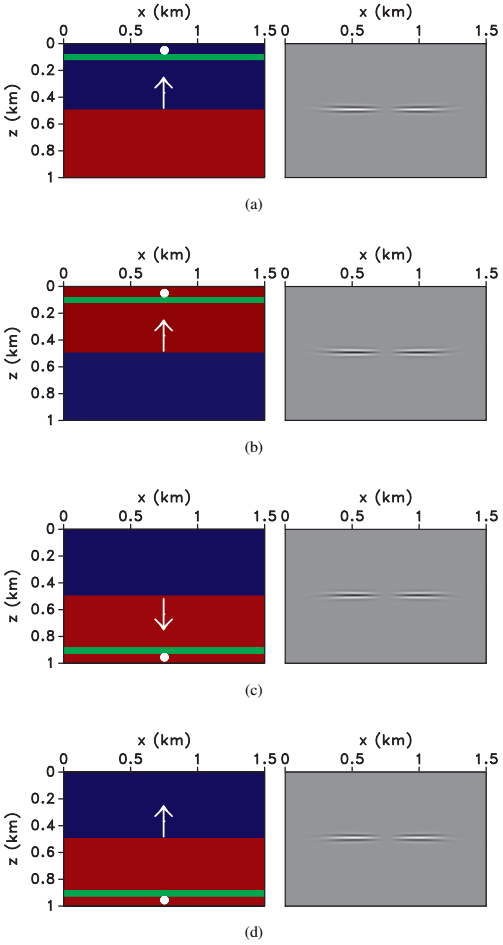

Figure 5: PS imaging of a horizontal interface for various source/receiver configurations. The left panels are the models with the acquisition geometry, and the right panels are the corresponding PS images. The dots are the locations of the sources and lines are the locations of the receivers. The arrow indicates the reflector normal for PS migration.

scalar imaging condition for the two cases shown in Figures 1 and 4 have the same polarity. This is because all reflector normal vectors are defined to point toward one side of the reflector (the vertical component of all normal vectors must have the same sign in order to avoid ambiguity). Thus, for the same type of incident P-modes, the signs of vector $\nabla P \times \mathbf{n}$ are opposite in the two cases depicted in Figures 1 and 4, because vectors ∇P points in opposite directions. The sign change of $\nabla P \times \mathbf{n}$ compensates for the difference in polarity of the reflected S-modes, and results in PS images having the same polarity regardless of the direction of the incident P-mode.

To further explain how the scalar imaging condition generates PS images with the same polarity for both cases depicted in Figures 1 and 4, we consider another synthetic example with one horizontal reflector, shown in Figures 5a-5d. The sources and receivers are positioned at the top of the first layer, and the reflector normal points upward. Using the elastic scalar imag-

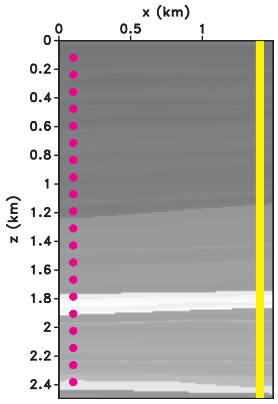

Figure 6: A crosswell example illustrating illumination for opposite sides of a reflector. The 20 sources, indicated by the dots, are in a well at $x = 0.1$ km. The receivers, indicated by the line, are at $x = 1.4$ km.

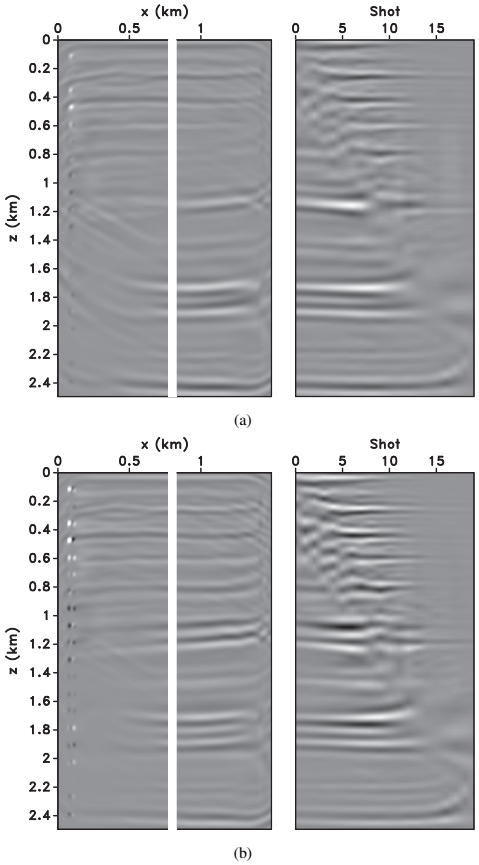

Figure 7: (a) The stacked PS image using conventional imaging condition. (b) The stacked PS image using the scalar imaging condition. The left panels are the stacked PS images and the right panels are common image gathers at $x = 0.8$ km.

ing condition, we obtain the PS image shown in Figure 5a. If we switch the material properties of the top and bottom layers while keeping the acquisition geometry and the direction of the reflector normal vector unchanged, we obtain the PS image shown in Figure 5b, which has opposite polarity compared to the image in Figure 5a. If we further rotate the entire experiment shown in Figure 5b by 180° or, equivalently, reverse the direction of the z-axis, we obtain the PS image shown in Figure 5c with the same polarity as the PS image shown in Figure 5b. Finally, by simply reversing the direction of the reflector normal from Figure 5c to Figure 5d, we obtain the PS image in Figure 5d with the same polarity as the image shown in Figure 5a. Notice that the only difference between the models shown in Figures 5a and 5d is that the incident P-modes illuminate the horizontal reflector from opposite sides. Therefore, using the scalar imaging condition, we obtain PS images of the same polarity for up-going and down-going waves.

We illustrate migration with waves approaching reflectors from opposite sides using a model consisting of gently dipping layers (Figure 6). The sources and receivers are in two wells. We use 20 sources evenly distributed in the well at $x = 0.1$ km, and 500 receivers located at $x = 1.4$ km. Using the conventional imaging condition, we obtain the PS image shown in the left panel of Figure 7a. The reflectors around $z = 1.2$ km are poorly imaged because they are illuminated by waves from opposite sides. In the common image gather at $x = 0.8$ km, the right panel of Figure 7a, the polarities of the events in different experiments are inconsistent. In contrast, Figure 7b shows the PS image using the scalar imaging condition. In this case, the interfaces in the image around $x = 1.4$ km are stronger, and the events have consistent polarities in all experiments, which confirms that the PS images computed using waves reflected at opposite sides of the reflector have consistent polarities.

CONCLUSIONS

Duan and Sava (2014) propose a scalar imaging condition for converted waves that corrects for polarity reversals in PS and SP images. The reflector normal is required for this imaging condition as prior information. In this paper, we discuss two practical problems of the scalar imaging condition. One is the estimation of reflector normals when the reflectors are imaged at incorrect positions. We show that it is more reliable to estimate reflector normals for PS and SP migration from stacked PS and SP images computed using conventional imaging methods. The other problem is imaging a reflector using waves from opposite sides. Using this imaging condition, we obtain converted wave images of consistent polarities when waves are reflected from opposite sides of a reflector, thus improving imaging quality and the robustness of the process.

ACKNOWLEDGMENTS

We thank the sponsors of the Center for Wave Phenomena, whose support made this research possible. The reproducible numeric examples in this paper use the Madagascar open-source software package (Fomel et al., 2013) freely available from http://www.ahay.org.

REFERENCES

Aki, K., and P. Richards, 2002, Quantitative seismology (second edition): University Science Books.

Artman, B., I. Podladtchikov, and A. Goertz, 2009, Elastic time-reverse modeling imaging conditions: SEG Technical Program Expanded Abstracts 2009, 1207–1211.

Dellinger, J., and J. Etgen, 1990, Wavefield separation in two-dimensional anisotropic media: Geophysicas, **55(7)**, 914–919.

Denli, H., and L. Huang, 2008, Elastic-wave reverse-time migration with a wavefield-separation imaging condition: SEG Technical Program Expanded Abstracts 2008, 2346–2350.

Duan, Y., and P. Sava, 2014, Converted-waves imaging condition for elastic reverse-time migration: SEG Technical Program Expanded Abstracts, 1904–1908.

Fomel, S., P. Sava, I. Vlad, Y. Liu, and V. Bashkardin, 2013, Madagascar: open-source software project for multidimensional data analysis and reproducible computational experiments: Journal of Open Research Software, **1**, e8.

MacLeod, M., R. Hanson, C.R.Bell, and S. McHugo, 1999, The Alba Field Ocean Bottom Cable Seismic Survey: Impact on Development: The Leading Edge, **18**, 1306–1312.

Mehta, K., D. Kiyashchenko, P. Jorgensen, J. Lopez, J. Ferrandis, and A. Mateeva, 2009, Advancements in processing and imaging of downhole multi-component data: SEG Technical Program Expanded Abstracts, 4299–4303.

Sen, M. K., 2009, Estimation of properties of shallow sediments from multi-component ocean bottom seismometer data: SEG Technical Program Expanded Abstracts, 4280–4281.

Versteeg, R., 1991, Analysis of the problem of the velocity model determination for seismic imaging: PhD thesis, University of Paris VII.

———, 1993, Sensitivity of prestack depth migration to the velocity model: Geophysics, **58**, 873–882.

Wu, R., R. Yan, and X, 2010, Elastic converted-wave path migration for subsalt imaging: SEG Technical Program Expanded Abstracts 2010, 3176–3180.

Yan, J., and P. Sava, 2008, Isotropic angle-domain elastic reverse-time migration: Geophysics, **73(6)**, S229–S239.